

## Direct evidence of the dominant role of multiphoton permanent-dipole transitions in strong-field dissociation of $\text{NO}^{2+}$

Bethany Jochim <sup>1,\*</sup> M. Zohrabi,<sup>1</sup> B. Gaire,<sup>1</sup> F. Anis,<sup>1</sup> Tereza Uhlíková,<sup>2</sup> K. D. Carnes,<sup>1</sup> E. Wells,<sup>3</sup> B. D. Esry,<sup>1</sup> and I. Ben-Itzhak<sup>1,†</sup>

<sup>1</sup>*J. R. Macdonald Laboratory, Department of Physics, Kansas State University, Manhattan, Kansas 66506, USA*

<sup>2</sup>*Department of Analytical Chemistry, University of Chemistry and Technology, Technická 5, 166 28 Praha 6, Czech Republic*

<sup>3</sup>*Department of Physics, Augustana University, Sioux Falls, South Dakota 57197, USA*



(Received 20 February 2022; accepted 21 March 2022; published 4 April 2022)

We study laser-induced dissociation of a metastable  $\text{NO}^{2+}$  ion-beam target into  $\text{N}^+ + \text{O}^+$ , focusing on the prominent contribution by molecules breaking parallel to the polarization at high peak laser intensity ( $\sim 10^{15}$  W/cm<sup>2</sup>). Our experimental results and time-dependent Schrödinger equation calculations show that, contrary to commonly held intuition that electronic transitions always prevail, the dominant process underlying this highly aligned dissociation is a multiphoton permanent-dipole transition involving only the electronic ground state and leading to its vibrational continuum. Strong-field permanent-dipole transitions should thus be considered generally, as they may play a significant role in other heteronuclear molecules. Moreover, their role should only grow in importance for longer wavelengths, a trending direction in ultrafast laser studies.

DOI: [10.1103/PhysRevA.105.043101](https://doi.org/10.1103/PhysRevA.105.043101)

### I. INTRODUCTION

Photochemical control is one goal at the heart of atomic, molecular, and optical physics [1–5]. Intense, femtosecond laser pulses possess fields comparable to the binding fields of molecules' valence electrons and temporal durations shorter than typical molecular vibration and rotational periods. As such, a multitude of studies over the past decades have established these pulses as promising tools for manipulating strong-field molecular processes and have gradually improved our understanding of them; see, e.g., reviews [2,4–9] and Refs. [10–17].

A framework for understanding the interactions of laser pulses with small molecules has been realized in studies of the simplest diatomic molecule,  $\text{H}_2^+$  [7,18]. All the main dissociative mechanisms in this benchmark system, bond softening [19], above-threshold dissociation (ATD) [20], etc., rely solely on the laser-induced coupling of different electronic states. Following the natural progression from simple to more complex, we build upon this framework to explore strong-field dynamics of multielectron molecules, applying the fundamental concepts developed in  $\text{H}_2^+$  studies. Among multielectron systems, heteronuclear molecules present intriguing complexities. For instance, their nonzero permanent dipole moments, created by the offset between their centers of mass and charge, allow transitions within the same electronic state to occur, opening up more pathways for dissociation and control.

Several theoretical studies have noted that permanent-dipole transitions can play an important role in strong-field dynamics [21–37]. While the wealth of theoretical results is

compelling, there has been little experimental consideration of strong-field-driven permanent-dipole transitions. Few experimental studies have highlighted strong-field permanent-dipole transitions, and the existing work has been controversial or did not present any direct evidence. For instance, Kiess *et al.* reported the first experimental evidence of permanent-dipole transitions in the benchmark heteronuclear diatomic molecule  $\text{HD}^+$  [38], but this measurement lacked the ability to distinguish H and D fragments. Utilizing a coincidence technique, McKenna *et al.* later attributed the same kinetic energy release (KER) peak to a one-photon bond softening mechanism, which does not involve the permanent dipole moment [39]. Recently, Wustelt *et al.* [40] attributed an intensity-dependent KER shift in  $\text{HeH}^+$  to stretching prior to ionization, which involves vibrational excitation of the electronic ground state. However, they were unable to measure dissociation, leaving open the question of whether the stretching occurred on the ground state or excited states, i.e., whether this dissociation mechanism is driven by the permanent dipole or not.

In many molecules, the permanent dipole moment is generally quite weak compared to the transition dipole moment [41]. In  $\text{HD}^+$ , discussed above, for example, the magnitude of the  $1s\sigma-2p\sigma$  transition dipole moment at the one-photon crossing in the light-dressed diabatic Floquet picture [42,43] is more than 3.5 times larger than the  $1s\sigma-1s\sigma$  permanent dipole moment at the internuclear distance relevant to the two-photon process proposed by Kiess *et al.* [44]. Hence, one might expect that permanent-dipole transitions have much smaller probabilities in comparison to electronic transitions. Indeed, in interpretation, it has generally become a common tendency to ignore permanent-dipole transitions in molecules in favor of electronic transitions; see, e.g., Refs. [45–58].

The lack of attention given to permanent-dipole transitions is perhaps due to the widespread use of Ti:sapphire (800 nm)

\*Corresponding author: [bjochim@phys.ksu.edu](mailto:bjochim@phys.ksu.edu)

†Corresponding author: [ibi@phys.ksu.edu](mailto:ibi@phys.ksu.edu)

laser light in experimental studies. With their 1.5 eV energy on the order of the electronic state spacing in typical diatomic molecules, 800-nm photons are typically inefficient at inciting and probing permanent dipole-driven dynamics. However, with the trend towards use of mid-infrared sources to enhance insight into tunneling ionization and high-harmonic generation [59], it is likely that permanent dipole-driven dynamics are increasingly relevant to strong-field molecular processes.

In this paper, we show clear experimental and theoretical evidence that the permanent dipole moment plays a key role in the main strong-field dissociation peaks of  $\text{NO}^{2+}$ . Specifically, we observe dominant permanent dipole-driven, three-photon transitions on the  $X^2\Sigma^+$  ground state, leading to dissociation into  $\text{N}^+ + \text{O}^+$ . The permanent dipole moments of dications tend to be larger than those of their neutral counterparts. In the present case, the ground state permanent dipole moment of  $\text{NO}^{2+}$  at the equilibrium internuclear distance is 0.75 a.u., whereas the corresponding quantity for NO is only 0.06 a.u. [60]. The larger permanent dipole moment of the dication makes it a good candidate for studying the impact of this property on strong-field dynamics.

## II. EXPERIMENTAL METHOD

In our experiment, a beam of  $\text{NO}^{2+}$  ions is produced by fast electron impact on vibrationally cold NO gas in an electron-cyclotron resonance (ECR) source and is accelerated to 9.2 keV, momentum analyzed, and focused by an electrostatic lens system. The resultant collimated  $0.9 \times 0.9$  mm<sup>2</sup> ion beam ( $\sim 0.5$  nA) travels to the laser interaction region, where this low density target (equivalent pressure of about  $2 \times 10^{-13}$  Torr at room temperature) is crossed by the laser beam. A multipass Ti:sapphire laser is used to produce 774-nm, 2-mJ, 27-fs pulses [full width at half maximum (FWHM) in intensity measured with second harmonic generation frequency-resolved optical gating (SHG FROG)] at 2 kHz. These pulses are focused onto the target ion beam by a 90° off-axis,  $f = 203$  mm parabolic mirror to a peak intensity of up to  $\sim 5 \times 10^{15}$  W/cm<sup>2</sup>. The laser intensity is evaluated by imaging the focus and is controlled in the experiment by changing the position of the focus relative to the center of the target ion beam (along the laser propagation direction) [61]. This method increases the interaction volume and allows us to maintain an  $\text{N}^+ + \text{O}^+$  coincidence rate of about 1 Hz even at the lower intensities. The laser-induced dissociation fragments carry a few keV of energy in the laboratory frame and are measured using a coincidence three-dimensional (3D) momentum imaging technique that has been described in detail in previous publications [62–64].

## III. $\text{NO}^{2+}$ TARGET PROPERTIES

In addition to its relatively strong permanent dipole moment, which is the main reason  $\text{NO}^{2+}$  was selected, the electronic structure properties of this molecular ion make it an attractive candidate for study. As  $\text{NO}^{2+}$  is metastable like many other molecular dications [65–67], only certain states survive from creation to interaction with the laser ( $\sim 20$   $\mu\text{s}$  travel time in our setup). The three lowest states of  $\text{NO}^{2+}$ ,  $X^2\Sigma^+$ ,  $A^2\Pi$ , and  $B^2\Sigma^+$ , shown in Fig. 1, as well as two

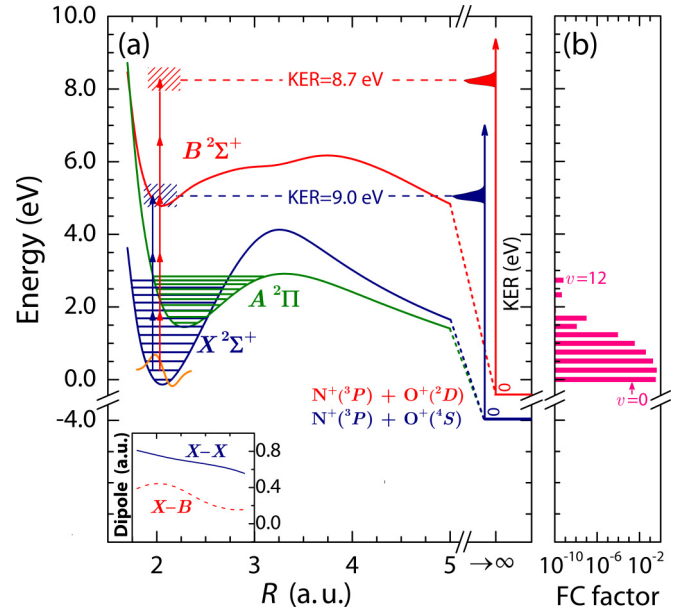


FIG. 1. (a) Lowest-lying doublet potential energy curves of  $\text{NO}^{2+}$ . The  $B^2\Sigma^+$  state dissociation limit is  $-0.42$  eV, and that of the  $X^2\Sigma^+$  and  $A^2\Pi$  states is  $-3.96$  eV, where zero is defined as  $v=0$  of  $X^2\Sigma^+$ . The arrows represent  $X^2\Sigma^+ \rightarrow X^2\Sigma^+$  (navy) and  $X^2\Sigma^+ \rightarrow B^2\Sigma^+$  (red) multiphoton transitions, both starting from  $v=1$ , whose schematic vibrational wave function is shown in orange. The navy and red hatched areas represent the vibrational continua of the  $X^2\Sigma^+$  and  $B^2\Sigma^+$  states, respectively. The schematic peaks with the corresponding colors on the right-hand side represent KER distributions for these bound-free pathways. The  $X^2\Sigma^+$  permanent dipole moment and  $X^2\Sigma^+ \rightarrow B^2\Sigma^+$  transition dipole moment are shown in the inset. (b) Franck-Condon (FC) population for the  $X^2\Sigma^+$  state of  $\text{NO}^{2+}$  resulting from  $\text{NO} \rightarrow \text{NO}^{2+}$  vertical electron impact ionization in the ion source followed by predissociation in flight to the interaction region.

higher-lying states,  $C^2\Sigma^+$  and  $c^4\Pi$ , are the only calculated states with bound potentials in the Franck-Condon region. The  $C^2\Sigma^+$  and  $c^4\Pi$  states fragment rapidly via tunneling or predissociation [68]. The  $A^2\Pi$  and  $B^2\Sigma^+$  states have predissociative, tunneling, and radiative lifetimes ranging from fractions of a microsecond to a few microseconds [69], leaving only the electronic ground state populated when probed by the laser.

Akin to  $\text{CO}^{2+}$ , which we have studied previously [57], the electronic ground state of  $\text{NO}^{2+}$  “cools” vibrationally via predissociation, specifically spin-orbit coupling with the  $A^2\Pi$  state [69]. Given the ion travel time mentioned above, this further limits the initial population to  $v = 0$ –12 of the  $X^2\Sigma^+$  state.

The laser field does not couple electronic states of differing spin, and the next-highest doublet state after  $B^2\Sigma^+$ ,  $2^2\Pi$  (not shown in Fig. 1), lies an additional 5 eV above the minimum of the  $B^2\Sigma^+$  state. Therefore, our  $\text{NO}^{2+}$  ion beam allows probing of the laser-induced response of a three-channel system. Moreover, the  $X^2\Sigma^+$  and  $A^2\Pi$  states are strongly coupled by one-photon transitions in a typical intense femtosecond laser pulse and are energetically well isolated

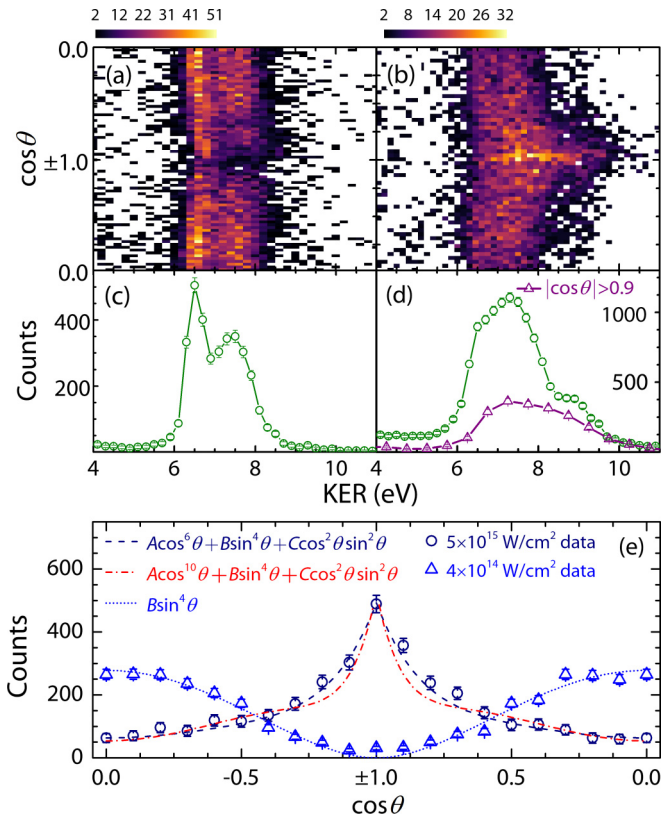


FIG. 2. (a) and (b) Density plots of  $\text{NO}^{2+} \rightarrow \text{N}^+ + \text{O}^+$  dissociation as a function of KER and  $\cos\theta$  for laser intensities  $4 \times 10^{14}$   $\text{W}/\text{cm}^2$  and  $5 \times 10^{15}$   $\text{W}/\text{cm}^2$ , respectively.  $\theta$  is the angle between the laser polarization and the  $\text{N}^+$  velocity vector. (c) and (d) One-dimensional KER plots of dissociation at laser intensities  $4 \times 10^{14}$   $\text{W}/\text{cm}^2$  and  $5 \times 10^{15}$   $\text{W}/\text{cm}^2$ , respectively. (e) Number of dissociation events as a function of  $\cos\theta$ . The  $5 \times 10^{15}$   $\text{W}/\text{cm}^2$  data, shown in navy, are for an 8.0–10.0 eV KER slice, and the  $4 \times 10^{14}$   $\text{W}/\text{cm}^2$  data, shown in blue, are for a 7.0–9.0 eV KER slice. The lines show functions fitted to the data, with horizontal error bars that are smaller than the symbols.

from the  $B^2\Sigma^+$  state. Hence,  $X^2\Sigma^+ \rightarrow A^2\Pi$  transitions are expected to dominate the dissociation.

To calculate the initial vibrational population of the  $\text{NO}^{2+}$  beam, shown in Fig. 1(b), we assume that the ions are produced via vertical transitions from the ground state of the neutral molecule to that of the dication [70]. The normalized vibrational state wave functions necessary for this analysis were calculated using a phase-amplitude method [71], yielding vibrational energies that are consistent with those of Baková *et al.* [69].

#### IV. RESULTS AND DISCUSSION

The main results of our measurements, of  $\text{NO}^{2+}$  dissociation to  $\text{N}^+ + \text{O}^+$  at two laser intensities, are shown in Fig. 2.

Lower intensity pulses ( $\leq 10^{15}$   $\text{W}/\text{cm}^2$ ) produce KER spectra with a two-peak structure, shown in panels (a) and (c), primarily resulting from dissociation perpendicular to the laser polarization, as expected for a  $\Delta\Lambda = 1$  transition [72]. As described in detail in our recent publication [73], the lower

KER peak is due to single photon excitation from the  $X^2\Sigma^+$  ground state to the  $A^2\Pi$  state followed by dissociation of the latter state. The higher KER peak is predominantly the result of two-photon absorption.

In contrast, higher intensity pulses ( $\sim 5 \times 10^{15}$   $\text{W}/\text{cm}^2$ ) yield a prominent highly aligned feature at  $|\cos\theta| = 1$ , shown in Figs. 2(b) and 2(e). Note that  $\theta$  is defined as the angle between the laser polarization and the  $\text{N}^+$  velocity vector. This highly aligned feature cannot come from  $X^2\Sigma^+ \rightarrow A^2\Pi$  transitions because a  $\Delta\Lambda = 1$  transition should exhibit an angular distribution peaked at  $|\cos\theta| = 0$ . Moreover, from Fig. 2(e), it is readily seen that there are two angular features in the different intensity regimes: (1) a sharp, aligned feature and (2) a distribution peaking at  $|\cos\theta| = 0$ . The aligned feature also extends to higher KER (8–11 eV), highlighted by the  $|\cos\theta| > 0.9$  slice in Fig. 2(d). This parallel, higher-KER part of the high-intensity data is our focus.

What are the underlying dynamics of this aligned feature? Following the dominant line of thought in the field, a purely electronic  $X^2\Sigma^+ \rightarrow B^2\Sigma^+$  transition would be a natural choice. Such a transition starting from the peak of the vibrational population ( $v = 1$ ) would produce 8.7 eV KER, as illustrated in Fig. 1(a), consistent with the data. Similar  $X^2\Sigma^+ \rightarrow B^2\Sigma^+$  transitions starting from neighboring vibrational levels can produce the remainder of the high-KER, highly aligned feature. As mentioned above, however, permanent-dipole transitions can also play an important role. An intriguing possibility is a three-photon vibrational excitation driven by the permanent dipole moment and involving solely the  $X^2\Sigma^+$  state. Starting from the peak of the Franck-Condon population, such a transition would produce 9.0 eV KER, shown schematically in Fig. 1(a), also consistent with our measurements.

The angular fits for the high intensity data in Fig. 2(e) shed some light on what dynamics are occurring. These support  $X^2\Sigma^+ \rightarrow X^2\Sigma^+$  transitions over  $X^2\Sigma^+ \rightarrow B^2\Sigma^+$  transitions. The fit function containing the  $\cos^6\theta$  term, which corresponds to a three-photon parallel transition, fits the data quite nicely, whereas the fit function containing the  $\cos^{10}\theta$  term, which corresponds to a five-photon parallel transition, is clearly too narrow and does not fit the data as well. It is important to note that the angular resolution,  $\delta$ , in our measurements is a function of the angle  $\theta$ , explicitly  $\delta(\cos\theta) \propto \sqrt{(1 - \cos^2\theta)}/\text{KER}$  [74], and it is best around  $\cos\theta = \pm 1$ , where the aligned feature peaks. As a side note, the  $\cos^2\theta \sin^2\theta$  term corresponds to a  $X^2\Sigma^+ \rightarrow X^2\Sigma^+ \rightarrow A^2\Pi$  pathway, i.e., a parallel one-photon permanent-dipole transition on the ground state followed by a perpendicular one-photon electronic transition to the first excited state.

While our experimental results strongly support the important role of permanent-dipole transitions, to further strengthen our claims, we solved the time-dependent Schrödinger equation (TDSE) in the Born-Oppenheimer representation [75]. The necessary potential energy curves, transition dipole moments, and permanent dipole moments were obtained by extending previous *ab initio* calculations [69]. These were computed using the complete active space self-consistent field (CASSCF) and internally contracted multireference configuration interaction (icMRCI) methods as implemented in

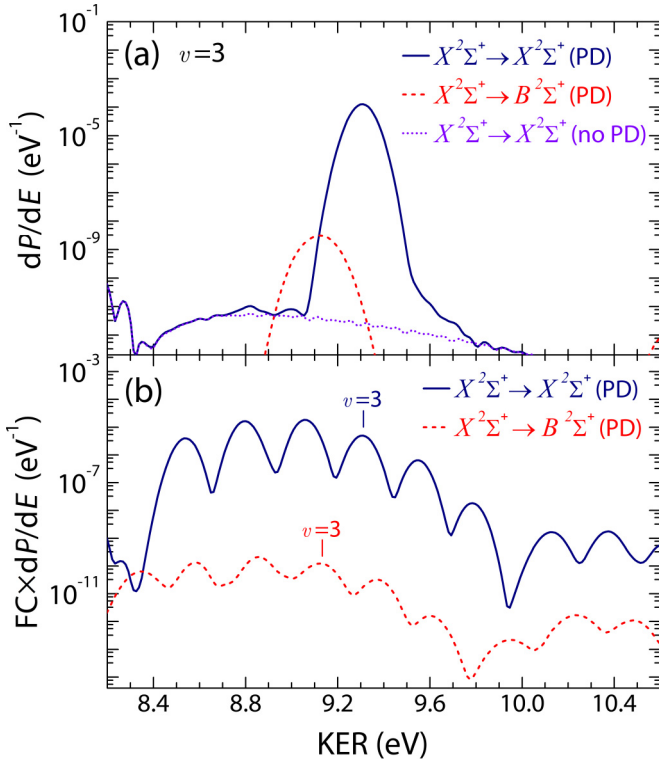


FIG. 3. Calculated KER spectra corresponding to (a) transitions starting at  $v = 3$  of the  $X^2\Sigma^+$  state and (b) transitions starting from  $v = 0-12$  weighted by their Franck-Condon factors. “PD” indicates that the permanent dipole moment is included, and “no PD” indicates that it is not included. Note that the  $X^2\Sigma^+ \rightarrow B^2\Sigma^+$  KER spectrum (no PD) is too small in amplitude to be seen on the graph ( $dP/dE \sim 10^{-14}$  eV<sup>-1</sup>). These calculations were performed at a laser intensity of  $10^{14}$  W/cm<sup>2</sup>.

the MOLPRO suite of programs [76]. The full active space consisted of  $1\sigma-6\sigma$ ,  $1\pi$ , and  $2\pi$  orbitals with all electrons correlated, and the Dunning correlation consistent basis set cc-pV6Z was used [77]. Relativistic corrections were carried out using the Douglas-Kroll-Hess Hamiltonian as implemented in MOLPRO [78–80]. The relativistic curves, which we included in our TDSE calculations, differ by no more than 0.1 eV from the uncorrected ones at any internuclear distance.

In the TDSE calculations, the three relevant electronic states ( $X^2\Sigma^+$ ,  $A^2\Pi$ , and  $B^2\Sigma^+$ ) were considered, with initial population in  $v = 0-12$  ( $J = 0$ ) of the  $X^2\Sigma^+$  state only. We performed our calculations at 800 nm wavelength and 35 fs pulse duration and repeated them at three intensities from  $5.0 \times 10^{13}$  to  $2.0 \times 10^{14}$  W/cm<sup>2</sup>. Vibration and nuclear rotation were included, but ionization was neglected [75]. Our calculations converged to about 1%.

The KER spectra obtained from our TDSE calculations are shown in Fig. 3. As can be seen in panel (a), theory predicts that  $X^2\Sigma^+ \rightarrow X^2\Sigma^+$  transitions are more likely than  $X^2\Sigma^+ \rightarrow B^2\Sigma^+$  transitions by about five orders of magnitude. Moreover, when the permanent dipole moment is not included in the calculation, the  $X^2\Sigma^+ \rightarrow X^2\Sigma^+$  peak vanishes, demonstrating that transitions driven by the permanent dipole moment lead to this aligned, high-KER feature.

Figure 3(a) also shows that the permanent dipole moment plays a key role in  $X^2\Sigma^+ \rightarrow B^2\Sigma^+$  transitions, as without the permanent dipole moment in the calculation, the  $X^2\Sigma^+ \rightarrow B^2\Sigma^+$  feature is also absent. It is also worth mentioning that the calculated transition probabilities, evaluated by integrating each probability density shown in Fig. 3(a), indicate that both the  $X^2\Sigma^+ \rightarrow X^2\Sigma^+$  (three-photon) and  $X^2\Sigma^+ \rightarrow B^2\Sigma^+$  (five-photon) transitions (explicitly having a probability of  $10^{-5}$  and  $5 \times 10^{-10}$ , respectively, for the initial  $v = 3$  state) are far from saturation in spite of the high intensity we used.

This dominance of  $X^2\Sigma^+ \rightarrow X^2\Sigma^+$  transitions over  $X^2\Sigma^+ \rightarrow B^2\Sigma^+$  transitions by several orders of magnitude persists even after Franck-Condon averaging over the initial vibrational population, as shown in Fig. 3(b). The vibrational structure seen in this calculated spectrum is not observed experimentally, as the resolution degrades with increasing KER. Specifically, at 9.0 eV KER, a conservative estimate of the resolution is 0.1 eV ( $1\sigma$ ) [63,81] for the present experimental conditions, which in conjunction with the laser bandwidth washes out the measured vibrational peaks.

One may wonder about the difference between the experimental and theoretical intensities. First, focal-volume averaging tends to lower the effective intensity of the experiment [43,82]. We note that under the conditions of our experiment the interaction volume exposed to low intensities is large [73]. Second, since including ionization in the theory is currently beyond reach, the calculations must be limited to intensities where ionization is acceptably small. We experimentally determined that this is true at  $1 \times 10^{14}$  W/cm<sup>2</sup> (<1% of dissociation), but it fails at  $1 \times 10^{15}$  W/cm<sup>2</sup> (~25% of dissociation) [73]. Thus, using intensities up to  $2 \times 10^{14}$  W/cm<sup>2</sup> in the theory is a reasonable compromise given these limitations.

The prevalence of  $X^2\Sigma^+ \rightarrow X^2\Sigma^+$  transitions over  $X^2\Sigma^+ \rightarrow B^2\Sigma^+$  transitions is due in large part to the lower number of photons required and the relative magnitudes of the dipole couplings. The dipole moments are shown in the inset in Fig. 1(a). At the internuclear distances near the  $X^2\Sigma^+$  minimum, the ratio of the  $X^2\Sigma^+$  permanent dipole moment to the  $X^2\Sigma^+ \rightarrow B^2\Sigma^+$  transition dipole moment is around 1.8 and relatively constant. Moreover, it is possible that the dominance of the permanent-dipole driven pathways is further enhanced by intermediate resonant transitions to highly excited vibrational levels of  $X^2\Sigma^+$ . For example, the  $\text{NO}^{2+}$  molecule can undergo resonant  $v = 1 \rightarrow v = 8$  and  $v = 8 \rightarrow v = 16$  photoexcitations before subsequently absorbing a final photon to arrive at the  $X^2\Sigma^+$  continuum.

Lastly, it is worth pointing out that our measurement technique and ion beam target choice draw a noteworthy distinction between our study and the sizable body of existing work on  $\text{NO}^{2+}$  [83–85]. The majority of the previous studies are noncoincidence and utilize a neutral NO initial target. An overarching conclusion of this previous work is that  $\text{N}^+$  and  $\text{O}^+$  fragments are mainly produced via indirect mechanisms that involve a series of dissociation and ionization steps. Starting with an  $\text{NO}^{2+}$  ion beam target likely reduces the number of intermediate states participating in the strong-field dynamics, and thus interpretation in our case is simpler and can potentially even involve fundamentally different physics.

## V. CONCLUSION

In summary, elucidation of the plausible dissociation pathways underlying the high intensity data from our experiment has proved to be an intriguing problem. Through the choice of a molecule that happens to have a strong permanent dipole moment, use of a powerful experimental method which affords us the ability to isolate this pathway experimentally via the KER and angular distributions, and theoretical support, we have demonstrated that the commonly overlooked permanent dipole moment can in some cases have a non-negligible and in fact dominating influence on the laser-induced dynamics, driving pathways involving a multiphoton vibrational excitation. With the field trending towards longer wavelengths and theory indicating that permanent-dipole transitions are important, this work will likely be a significant factor for strong-field physics researchers to consider in the future.

## ACKNOWLEDGMENTS

The authors acknowledge C. W. Fehrenbach for his ion beam expertise and Z. Chang's and V. Kumarappan's groups for assistance with the laser beam. This work was supported by the Chemical Sciences, Geosciences, and Biosciences Division, Office of Basic Energy Sciences, Office of Science, U.S. Department of Energy under Grant No. DE-FG02-86ER13491. B.J. was also supported by the Department of Energy Office of Science Graduate Fellowship Program (DOE SCGF), made possible in part by the American Recovery and Reinvestment Act of 2009, administered by ORISE-ORAU under Contract No. DE-AC05-06OR23100. T.U. acknowledges computational resources provided by the ELIXIR-CZ (LM2018131) and e-Infrastruktura CZ (e-INFRA LM2018140) project. E.W. was supported by National Science Foundation Grant No. PHY-2011864.

- 
- [1] P. Brumer and M. Shapiro, *Annu. Rev. Phys. Chem.* **43**, 257 (1992).
- [2] A. Zewail, *Pure Appl. Chem.* **72**, 2219 (2000).
- [3] M. Shapiro and P. Brumer, *Rep. Prog. Phys.* **66**, 859 (2003).
- [4] P. Nuernberger, G. Vogt, T. Brixner, and G. Gerber, *Phys. Chem. Chem. Phys.* **9**, 2470 (2007).
- [5] D. Keefer and R. de Vivie-Riedle, *Acc. Chem. Res.* **51**, 2279 (2018).
- [6] T. Brixner and G. Gerber, *Chem. Phys. Chem.* **4**, 418 (2003).
- [7] J. H. Posthumus, *Rep. Prog. Phys.* **67**, 623 (2004).
- [8] M. Dantus and V. V. Lozovoy, *Chem. Rev.* **104**, 1813 (2004).
- [9] I. V. Hertel and W. Radloff, *Rep. Prog. Phys.* **69**, 1897 (2006).
- [10] R. S. Judson and H. Rabitz, *Phys. Rev. Lett.* **68**, 1500 (1992).
- [11] A. Assion, T. Baumert, M. Bergt, T. Brixner, B. Kiefer, V. Seyfried, M. Strehle, and G. Gerber, *Science* **282**, 919 (1998).
- [12] R. J. Levis, G. M. Menkir, and H. Rabitz, *Science* **292**, 709 (2001).
- [13] T. Ergler, A. Rudenko, B. Feuerstein, K. Zrost, C. D. Schröter, R. Moshhammer, and J. Ullrich, *Phys. Rev. Lett.* **97**, 193001 (2006).
- [14] A. Hishikawa, A. Matsuda, M. Fushitani, and E. J. Takahashi, *Phys. Rev. Lett.* **99**, 258302 (2007).
- [15] D. Geißler, P. Marquetand, J. González-Vázquez, L. González, T. Rozgonyi, and T. Weinacht, *J. Phys. Chem. A* **116**, 11434 (2012).
- [16] U. Lev, L. Graham, C. B. Madsen, I. Ben-Itzhak, B. D. Bruner, B. D. Esry, H. Frostig, O. Heber, A. Natan, V. S. Prabhudesai, D. Schwalm, Y. Silberberg, D. Strasser, I. D. Williams, and D. Zajfman, *J. Phys. B* **48**, 201001 (2015).
- [17] M. Nairat, V. V. Lozovoy, and M. Dantus, *J. Phys. Chem. A* **120**, 8529 (2016).
- [18] H. Ibrahim, C. Lefebvre, A. D. Bandrauk, A. Staudte, and F. Légaré, *J. Phys. B* **51**, 042002 (2018).
- [19] P. H. Bucksbaum, A. Zavriyev, H. G. Muller, and D. W. Schumacher, *Phys. Rev. Lett.* **64**, 1883 (1990).
- [20] A. Giusti-Suzor, X. He, O. Atabek, and F. H. Mies, *Phys. Rev. Lett.* **64**, 515 (1990).
- [21] A. Kondo, W. J. Meath, S. H. Nilar, and A. J. Thakkar, *Chem. Phys.* **186**, 375 (1994).
- [22] A. Datta, S. Saha, and S. S. Bhattacharyya, *J. Phys. B* **30**, 5737 (1997).
- [23] A. Conjusteau, A. D. Bandrauk, and P. B. Corkum, *J. Chem. Phys.* **106**, 9095 (1997).
- [24] C. M. Dion, A. Keller, O. Atabek, and A. D. Bandrauk, *Phys. Rev. A* **59**, 1382 (1999).
- [25] A. Kondorskiy and H. Nakamura, *Phys. Rev. A* **66**, 053412 (2002).
- [26] J. T. Paci, D. M. Wardlaw, and A. D. Bandrauk, *J. Phys. B* **36**, 3999 (2003).
- [27] G. L. Kamta and A. D. Bandrauk, *Phys. Rev. Lett.* **94**, 203003 (2005).
- [28] W. J. Meath, *J. Opt. Soc. Am. B* **25**, 865 (2008).
- [29] N. Elghobashi-Meinhardt, L. González, I. Barth, and T. Seideman, *J. Chem. Phys.* **130**, 024310 (2009).
- [30] D. Ursrey, F. Anis, and B. D. Esry, *Phys. Rev. A* **85**, 023429 (2012).
- [31] Q. Su, Y. Han, and S.-L. Cong, *J. Chem. Phys.* **138**, 024304 (2013).
- [32] E. Dehghanian, A. D. Bandrauk, and G. Lagmago Kamta, *J. Chem. Phys.* **139**, 084315 (2013).
- [33] E. de Lima, E. Rosado, L. Castelano, and R. E. de Carvalho, *Phys. Lett. A* **378**, 2657 (2014).
- [34] A. Nikodem, R. D. Levine, and F. Remacle, *J. Phys. Chem. A* **120**, 3343 (2016).
- [35] V.-H. Hoang, S.-F. Zhao, V.-H. Le, and A.-T. Le, *Phys. Rev. A* **95**, 023407 (2017).
- [36] D. Ursrey and B. D. Esry, *Phys. Rev. A* **96**, 063409 (2017).
- [37] L. Yue, P. Wustelt, A. M. Sayler, F. Oppermann, M. Lein, G. G. Paulus, and S. Gräfe, *Phys. Rev. A* **98**, 043418 (2018).
- [38] A. Kiess, D. Pavičić, T. W. Hänsch, and H. Figger, *Phys. Rev. A* **77**, 053401 (2008).
- [39] J. McKenna, A. M. Sayler, B. Gaire, N. G. Johnson, M. Zohrabi, K. D. Carnes, B. D. Esry, and I. Ben-Itzhak, *J. Phys. B* **42**, 121003 (2009).
- [40] P. Wustelt, F. Oppermann, L. Yue, M. Möller, T. Stöhlker, M. Lein, S. Gräfe, G. G. Paulus, and A. M. Sayler, *Phys. Rev. Lett.* **121**, 073203 (2018).

- [41] *Coherent Control of Molecules*, edited by B. Lasorne and G. Worth (Collaborative Computational Project on Molecular Quantum Dynamics (CCP6), Daresbury, 2006).
- [42] A. Giusti-Suzor, F. H. Mies, L. F. DiMauro, E. Charron, and B. Yang, *J. Phys. B* **28**, 309 (1995).
- [43] *Molecules and Clusters in Intense Laser Fields*, edited by J. Posthumus (Cambridge University Press, Cambridge, 2001).
- [44] B. D. Esry and H. R. Sadeghpour, *Phys. Rev. A* **60**, 3604 (1999).
- [45] J. Lavancier, D. Normand, C. Cornaggia, J. Morellec, and H. X. Liu, *Phys. Rev. A* **43**, 1461 (1991).
- [46] C. Cornaggia, J. Lavancier, D. Normand, J. Morellec, P. Agostini, J. P. Chambaret, and A. Antonetti, *Phys. Rev. A* **44**, 4499 (1991).
- [47] P. Dietrich and P. B. Corkum, *J. Chem. Phys.* **97**, 3187 (1992).
- [48] K. Codling and L. J. Frasinski, *J. Phys. B* **26**, 783 (1993).
- [49] M. Stankiewicz, L. J. Frasinski, G. M. Cross, P. A. Hatherly, K. Codling, A. J. Langley, and W. Shaikh, *J. Phys. B* **26**, 2619 (1993).
- [50] S. M. Hankin, D. M. Villeneuve, P. B. Corkum, and D. M. Rayner, *Phys. Rev. Lett.* **84**, 5082 (2000).
- [51] S. A. Hosseini and D. Goswami, *Phys. Rev. A* **64**, 033410 (2001).
- [52] S. M. Hankin, D. M. Villeneuve, P. B. Corkum, and D. M. Rayner, *Phys. Rev. A* **64**, 013405 (2001).
- [53] E. Wells, M. J. DeWitt, and R. R. Jones, *Phys. Rev. A* **66**, 013409 (2002).
- [54] J. Wu, H. Zeng, and C. Guo, *J. Phys. B* **39**, 3849 (2006).
- [55] J. Wu, H. Zeng, and C. Guo, *J. Phys. B* **40**, 1095 (2007).
- [56] P. A. Orr, I. D. Williams, J. B. Greenwood, I. C. E. Turcu, W. A. Bryan, J. Pedregosa-Gutierrez, and C. W. Walter, *Phys. Rev. Lett.* **98**, 163001 (2007).
- [57] J. McKenna, A. M. Sayler, F. Anis, N. G. Johnson, B. Gaire, U. Lev, M. A. Zohrabi, K. D. Carnes, B. D. Esry, and I. Ben-Itzhak, *Phys. Rev. A* **81**, 061401(R) (2010).
- [58] M. Kotur, T. C. Weinacht, C. Zhou, and S. Matsika, *Phys. Rev. X* **1**, 021010 (2011).
- [59] C. Vozzi, M. Negro, and S. Stagira, *J. Mod. Opt.* **59**, 1283 (2012).
- [60] R. D. Nelson, Jr., D. R. Lide, Jr., and A. A. Maryott, *Selected Values of Electric Dipole Moments for Molecules in the Gas Phase* (U.S. National Bureau of Standards, Washington, 1967).
- [61] A. M. Sayler, P. Q. Wang, K. D. Carnes, and I. Ben-Itzhak, *J. Phys. B: At., Mol. Opt. Phys.* **40**, 4367 (2007).
- [62] I. Ben-Itzhak, P. Q. Wang, J. F. Xia, A. M. Sayler, M. A. Smith, K. D. Carnes, and B. D. Esry, *Phys. Rev. Lett.* **95**, 073002 (2005).
- [63] P. Q. Wang, A. M. Sayler, K. D. Carnes, J. F. Xia, M. A. Smith, B. D. Esry, and I. Ben-Itzhak, *Phys. Rev. A* **74**, 043411 (2006).
- [64] A. M. Sayler, Measurements of ultrashort intense laser-induced fragmentation of simple molecular ions, Ph.D. thesis, Kansas State University, 2008.
- [65] D. Mathur, *Phys. Rep.* **225**, 193 (1993), and references therein.
- [66] D. Mathur, *Phys. Rep.* **391**, 1 (2004).
- [67] S. D. Price, *Int. J. Mass Spectrom.* **260**, 1 (2007), and references therein.
- [68] D. Edvardsson, M. Lundqvist, P. Baltzer, B. Wannberg, and S. Lunell, *Chem. Phys. Lett.* **256**, 341 (1996).
- [69] R. Baková, J. Fišer, T. Šedivcová-Uhlíková, and V. Špirko, *J. Chem. Phys.* **128**, 144301 (2008).
- [70] Z. Amitay, A. Baer, M. Dahan, J. Levin, Z. Vager, D. Zajfman, L. Knoll, M. Lange, D. Schwalm, R. Wester, A. Wolf, I. F. Schneider, and A. Suzor-Weiner, *Phys. Rev. A* **60**, 3769 (1999).
- [71] E. Y. Sidky and I. Ben-Itzhak, *Phys. Rev. A* **60**, 3586 (1999).
- [72] A. M. Sayler, P. Q. Wang, K. D. Carnes, B. D. Esry, and I. Ben-Itzhak, *Phys. Rev. A* **75**, 063420 (2007).
- [73] B. Jochim, M. Zohrabi, B. Gaire, T. Uhlíková, K. D. Carnes, E. Wells, B. D. Esry, and I. Ben-Itzhak, *Phys. Rev. A* **104**, 053112 (2021).
- [74] I. Ben-Itzhak, P. Wang, J. Xia, A. Max Sayler, M. A. Smith, J. Maseberg, K. D. Carnes, and B. D. Esry, *Nucl. Instrum. Methods Phys. Res. Sect. B* **233**, 56 (2005); note that the sign in the  $\cos \theta$  error expression should be minus and not a plus.
- [75] F. Anis and B. D. Esry, *Phys. Rev. A* **77**, 033416 (2008).
- [76] H.-J. Werner, P. J. Knowles, G. Knizia, F. R. Manby, M. Schütz *et al.*, Molpro, version 2012.1, a package of ab initio programs, 2012, <http://www.molpro.net>.
- [77] T. H. Dunning, *J. Chem. Phys.* **90**, 1007 (1989).
- [78] M. Douglas and N. M. Kroll, *Ann. Phys. (NY)* **82**, 89 (1974).
- [79] B. A. Hess, *Phys. Rev. A* **32**, 756 (1985).
- [80] B. A. Hess, *Phys. Rev. A* **33**, 3742 (1986).
- [81] B. Gaire, Imaging of slow dissociation of the laser induced fragmentation of molecular ions, Ph.D. thesis, Kansas State University, 2011.
- [82] J. J. Hua and B. D. Esry, *Phys. Rev. A* **78**, 055403 (2008).
- [83] A. Talebpour, S. Larochelle, and S. L. Chin, *J. Phys. B* **30**, 1927 (1997).
- [84] C. Guo and K. Wright, *Phys. Rev. A* **71**, 021404(R) (2005).
- [85] C. Guo, *J. Phys. B* **38**, L323 (2005).